Received September 14, 2019, accepted October 2, 2019, date of publication October 7, 2019, date of current version October 22, 2019.

Digital Object Identifier 10.1109/ACCESS.2019.2945990

Hybrid Photovoltaic-Thermoelectric Generator Powered Synchronous Reluctance Motor for Pumping Applications

MOHAMED N. IBRAHIM[1,2,3], HEGAZY REZK[4,5], MUJAHED AL-DAHIFALLAH[6], AND PETER SERGEANT[1,2], (Senior Member, IEEE)

[1]Department of Electrical Energy, Metals, Mechanical Constructions and Systems, Ghent University, 9000 Ghent, Belgium
[2]FlandersMake@UGent – corelab EEDT-MP, 3001 Leuven, Belgium
[3]Electrical Engineering Department, Kafrelshiekh University, Kafr el-Sheikh 33511, Egypt
[4]College of Engineering at Wadi Addawaser, Prince Sattam Bin Abdulaziz University, Wadi Aldawaser 11991, Saudi Arabia
[5]Electrical Engineering Department, Faculty of Engineering, Minia University, Minia 61111, Egypt
[6]Systems Engineering Department, King Fahd University of Petroleum and Minerals, Dhahran 31261, Saudi Arabia

Corresponding authors: Mohamed N. Ibrahim (m.nabil@ugent.be) and Mujahed Al-Dahifallah (mujahed@kfupm.edu.sa)

This work was supported in part by the Ghent University, and in part by the King Fahd University of Petroleum and Minerals.

ABSTRACT The interest in photovoltaic (PV) pumping systems has increased, particularly in rural areas where there is no grid supply available. However, both the performance and the cost of the whole system are still an obstacle for a wide spread of this technology. In this article, a hybrid photovoltaic (PV)-thermoelectric generator (TEG) is investigated for pumping applications. The electric drivetrain comprises a synchronous reluctance motor and an inverter. A control strategy for the drivetrain is employed to execute two main tasks: 1) driving the motor properly to achieve a maximum torque per Ampère condition and 2) maximizing the output power of the PV system at different weather conditions. This means that the conventional DC-DC converter is not used in the proposed system. Moreover, batteries, which are characterized by short life expectancy and high replacement cost, are also not used. It is found that the motor output power and the pump flow rate are increased by about 9.5% and 12% respectively when the hybrid PV-TEG array is used compared to only using PV array. Accordingly, the performance, cost and complexity of the system are improved. Measurements on an experimental laboratory setup are constructed to validate the theoretical results of this work.

INDEX TERMS Photovoltaic pumping system, thermoelectric generator, MPPT, synchronous reluctance machines, motor drives.

I. INTRODUCTION

In the last decades, the global warming has become a major issue. In addition, the prices of the fossil fuel has also increased significantly. Therefore, there is an increased demand on using the renewable energy sources to cover the world need of electricity and to reduce the dependence on the fossil fuel [1], [2]. Solar energy is completely free, accessible by everyone and inexhaustible. The Sun light can be converted directly to electric energy by using photovoltaic (PV) cells. However, this conversion process has a low efficiency and high capital cost. Several progress in this field has been made to increase the efficiency and to minimize the cost of the energy produced by the PV systems [1]–[5].

The associate editor coordinating the review of this manuscript and approving it for publication was Zhuang Xu.

In rural areas, where no possibility to receive an electricity from the grid, the PV standalone systems have been become a promising solution compared to the traditional methods like diesel generation systems. This is thanks to several merits, among them the reduction in the PV modules price, no noise, low running cost and low cost or almost free maintenance [1], [2]. PV arrays convert directly the sun irradiation to electric energy that can be consumed in home appliances, lighting and pumping water for human needs and agriculture. However, the PV array has a low efficiency i.e. between 4-18% depending on the components of the PV cell. This results in a lower efficiency of the whole PV system. Therefore, there is a necessity to increase the harvested energy from PV arrays in order to enhance the performance of the whole system [2], [3].

The PV cells convert only a small amount of the incident solar irradiation to electric energy. The remainder part of solar irradiation is converted to heat, resulting in an increased PV cell temperature: up to 40 °C above the ambient temperature [4]. The harvested energy from the PV cells reduces with the higher cell temperature; hence, a cooling system is sometimes mandatory [6]. Instead of installing a cooling system for the PV arrays that could increase the whole system cost, thermoelectric generator (TEG) modules to convert the generated heat from the PV cell to electrical energy could be a promising solution. The TEG modules are mounted in the backside of the PV modules to form the so-called ''hybrid PV-TEG array'' [4]–[6].

In the literature, various research work has been presented about the hybrid PV-TEG system, for example, [1], [4], [5], [7]. In [1], it is proved that using the heat from the PV panel to generate electricity using the TEG is possible. In addition, both PV and TEG arrays are connected in parallel to feed a resistive load and a battery. The output power of each of both arrays is maximized for the different operating conditions. However, this hybrid system has two DC-DC converters with two controllers to increase the harvested energy from the arrays, which increase the cost and complexity of the system. The theoretical assessment of the hybrid PV-TEG system is shown in [5] based on the commercial data of the PV and TEG modules. It is shown that the integration of PV and TEG leads to an increased efficiency and output power compared to the standalone PV system: about 5% and 6% respectively. The performance of hybrid PV-TEG system is investigated in [7] via a thermodynamic approach. The effect of different conditions and structures of both PV and TEG modules is reported. It is found that the hybrid PV-TEG system has a higher output power, an improved efficiency and a lower emission of the wasted heat.

In the PV systems, it is recommended to use maximum power point tracking (MPPT) technique for maximizing the harvested output power of the PV arrays. Several MPPT methods have been presented in the literature e.g. perturbation and observation technique etc. [8], [9]. Maximizing the output power of the PV array is often done by introducing a DC-DC converter. By modifying the duty ratio of the converter, the impedance that is seen by the PV array will be varied and hence their maximum available power could be extracted [10]–[13]. Further, in the PV pumping system, it is also possible to maximize the output power of the PV system using only the inverter that drives the electric motor, without introducing additional DC-DC converter. The maximum power of the PV array is extracted by controlling the motor inverter [14]–[18]. Thus, there is no need for a DC-DC converter.

In the PV pumping system, many types of electric motors have been employed, starting from the early direct current (DC) motors to the recent various types of alternating current (AC) motors. The DC motors have the well-known disadvantages of using brushes and commutators, which require a frequently maintenance and thus a running cost. Consequently, they are rare to be used in the recent days. Several types of AC motors are used in the PV pumping system such as induction motors, brushless direct current motors, switched reluctance motors, permanent magnets synchronous motors and recently synchronous reluctance motors [13], [14]. Each motor has its own advantages and disadvantages among them the cost, the control, the converter, and the size. Synchronous reluctance motors (SynRMs) have been receiving a great interest in variable speed drive applications such as pumping systems. This is thanks to their several merits such as no magnets and windings/cages in the rotor and they use the conventional stator and drive system of the conventional electric machines e.g. induction motors. Consequently, they have a much better efficiency than the induction machines and less or comparable cost compared to the other types of AC machines [19]–[22].

To the best of the author's knowledge, there is no research work presented in the literature about the hybrid PV-TEG system when connected to SynRM for pumping application. This article investigates the performance of the hybrid PV-TEG array supplied SynRM for pumping applications. The system has neither batteries nor DC-DC converters. The maximum power tracking of the hybrid PV-TEG system is done by a proposed control strategy for the motor inverter. Eventually, the proposed system has an improved performance and could be a promising solution for pumping applications in remote areas.

II. SYSTEM DESCRIPTION

The system under study consists of PV modules, TEG modules, three phase voltage source inverter, three phase SynRM, centrifugal pump and control system as sketched in Fig. 1. The TEG modules are installed directly at the backside of the PV modules as seen in Fig. 1 (bottom).

In order to investigate the performance of the whole system, the mathematical model of the different components is necessary. The complete mathematical model is presented in [15]–[19] and briefly mentioned here.

A. PV MODULE MODEL

The PV module is represented by a single diode with series and parallel resistances, as sketched in Fig. 2.

The current-voltage (I_{ph}-V_{ph}) behavior of the PV module is given by [3], [4]:

$$I_{PV} = \left(I_{ph} - I_o \left[\exp\left(\frac{V_{PV} + R_s I_{PV}}{V_t a} \right) - 1 \right] - \frac{V_{PV} + R_s I_{PV}}{R_p} \right) \quad (1)$$

where:

I_{pv}:	The current	I_o:	The saturation current
V_{pv}:	The voltage	I_{ph}:	The photo current
V_t:	The thermal voltage	R_s:	The series resistance
a:	The diode ideality factor	R_p:	The parallel resistance

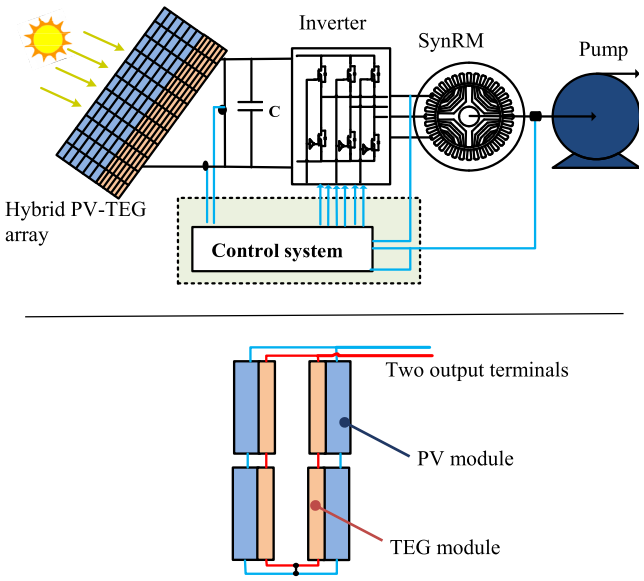

FIGURE 1. (Top) Hybrid PV-TEG pumping system, and (Bottom) an example of series wiring connection of PV array (2 series modules and 2 parallel strings) and TEG array (2 series and 2 parallel strings).

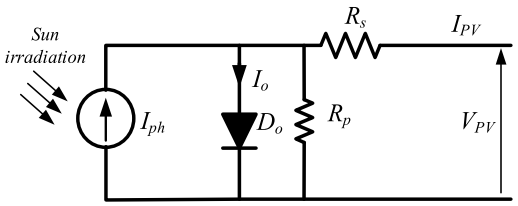

FIGURE 2. Equivalent circuit of the PV module.

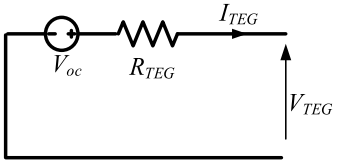

FIGURE 3. Equivalent circuit of the TEG module.

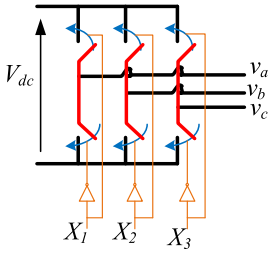

FIGURE 4. Equivalent circuit of the VSI module.

B. TEG MODULE MODEL

The basic unit of a TEG is the thermocouple, which consists of a couple of a P-type and a N-type pellets interconnected by a metal. It comprises of thermocouples arrays, which are connected in series to increase the operating voltage and in parallel to decrease the thermal resistance. Further, it is sandwiched between two ceramic heat exchanger plates for uniform thermal expansion. The simple basic model of the TEG module is represented by the following equation [4]–[7]:

$$V_{TEG} = V_{oc} - R_{TEG} \times I_{TEG} \tag{2}$$

where V_{oc} is the open circuit voltage which depends on the Seebeck effect and the temperature difference between the hot and cold sides of the *TEG* module; R_{TEG} and I_{TEG} are the internal resistance and current of the TEG module respectively.

The open-circuit voltage V_{oc} is obtained from the following equation:

$$V_{oc} = \alpha \times (T_h - T_C) = \alpha \times DT \tag{3}$$

where T_h and T_c are the temperatures of the hot and cold sides; DT is the temperature difference across the two junctions; α denotes the Seebeck coefficient.

C. THREE PHASE VOLTAGE SOURCE INVERTER

The three phase voltage source inverter (*VSI*) is modelled by the relation between the input *DC* bus voltage (V_{dc}) and the output voltage of the three phases (v_{an}, v_{bn} and v_{cn}). This relation is governed by the status of the IGBT switches (X_1, X_2 and X_3) as follows [9]:

$$\begin{bmatrix} v_{an} \\ v_{bn} \\ v_{cn} \end{bmatrix} = \frac{V_{dc}}{3} \begin{bmatrix} 2 & -1 & -1 \\ -1 & 2 & -1 \\ -1 & -1 & 2 \end{bmatrix} \begin{bmatrix} X_1 \\ X_2 \\ X_3 \end{bmatrix} \tag{4}$$

D. THREE PHASE SYNRM MODEL

It is common to model the AC machines in the *dq*-axis reference frame to avoid the variation of the inductance with time. However, in SynRMs, the *dq*-axis inductances vary with the *dq*-axis current components. This variation is well-known as the magnetic saturation effect. It is proved in [19] that the magnetic saturation influence on the inductances of the SynRM must be considered in the model for a correct prediction of SynRM performance. The accurate SynRM model is presented in [19] and it is used in this work. The equivalent *dq*-axis circuit of SynRM is shown in Figure 5 and the main

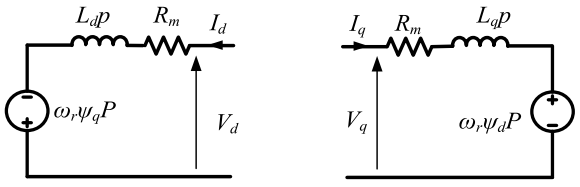

FIGURE 5. Equivalent circuit of the SynRM.

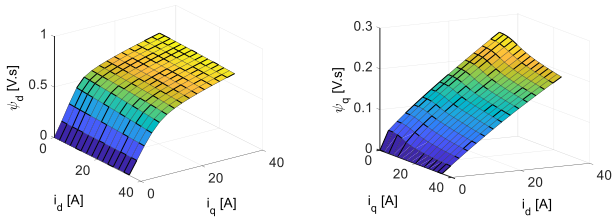

FIGURE 6. Flux-linkage components of the SynRM versus the current components.

governing equations are as follows:

$$\left.\begin{aligned}
&\begin{bmatrix} v_d \\ v_q \end{bmatrix} = \begin{bmatrix} R_m & 0 \\ 0 & R_m \end{bmatrix} \begin{bmatrix} i_d \\ i_q \end{bmatrix} + \begin{bmatrix} p & -\omega_r P \\ \omega_r P & p \end{bmatrix} \begin{bmatrix} \psi_d \\ \psi_q \end{bmatrix} \\
&T_e = \frac{3}{2} P(\psi_d i_q - \psi_q i_d) \\
&\psi_d = L_d(i_d, i_q) i_d \\
&\psi_q = L_q(i_d, i_q) i_q \\
&T_e = J \frac{d\omega_r}{dt} + B\omega_r + T_L
\end{aligned}\right\} \quad (5)$$

where:

v:	The voltage	d, q:	The direct and quadrature axis components respectively
i:	The current	R_m:	The stator phase resistance
ψ, L:	The flux linkage and the inductance respectively	P, p:	The pole pairs and the differential operator respectively
T_e:	The SynRM torque	J, B:	The moment of inertia and viscous coefficient of the system respectively
T_L:	The load torque	ω_r:	The rotor mechanical speed

The magnetic saturation influence on the dq-axis flux linkages of the machine is taken into account in (4). This can be done by either measurements or finite element modelling (FEM). Here, the FEM is used to obtain the influence of the magnetic saturation on the dq-axis flux linkages. This is included in (4) by lookup tables (LUTs) for the dq-axis flux linkages as function of the dq-axis current components as reported in Figure 6.

E. CENTRIFUGAL PUMP MODEL

The centrifugal pump (cp) is modelled by its torque-speed curve as follows:

$$T_{cp} = K_p \omega_r^2 \quad (6)$$

T_{cp} represents T_L in (4).

III. CONTROL SYSTEM

As mentioned in the introduction that in the PV-TEG system mostly two MPPT schemes based on two DC-DC converters are employed to maximize the output power of the PV and TEG arrays. In contrast, in this paper, only one MPPT scheme is integrated with the motor control technique to drive the motor inverter to execute two tasks: 1) driving the motor properly and 2) maximizing the output power of the hybrid PV-TEG system at different weather conditions. This means that no DC-DC converters are used.

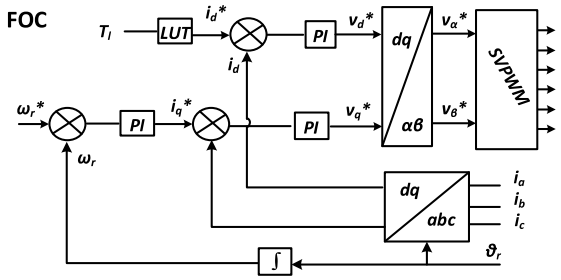

FIGURE 7. Representation diagram of the field oriented control (FOC) technique.

In the proposed system, the control part plays a very essential role in the whole system performance. The operating point of both the hybrid PV-TEG system and the motor depend on the control and thus the performance of the whole system is affected accordingly. Firstly, there are several methods to control the SynRM so that it achieves a condition of maximum torque per Ampère (MTA), maximum power factor (MPF), minimum losses (MLs) or maximum efficiency (ME). In this work, the MTA condition is used in SynRM. To do so, the field oriented control (FOC) method is used to drive the motor inverter so that the SynRM works at the MTA condition. Representation diagram of the FOC technique is presented in Fig. 7. The MTA condition is achieved in the FOC technique based on a lookup table (LUT) that is generated from FEM. This table correlates the d-axis current set point component (i_d^*) as a function of the required load torque. The speed set point of the FOC is however obtained from the MPPT control of the PV-TEG system, see Fig. 5. Secondly, In order to extract the maximum available power of the hybrid PV-TEG array, a MPPT approach is necessary. The perturbation and observation (P&O) MPPT scheme is employed. Figure 8 displays the schematic diagram of the perturbation and observation (P&O) MPPT scheme. It is obvious from Figure 8 that the measured voltage and current of the PV array are the inputs of the P&O scheme while the speed set point of the motor FOC is the output. Figure 9 shows the complete schematic diagram of the whole system.

IV. BEHAVIOR OF THE PV-TEG ARRAY

As mentioned before that the proposed system has no DC-DC converter. Consequently, it is essential to understand the behavior of both PV and TEG arrays so that the optimal connection can be made to be able to maximize the power of both arrays using only the motor inverter.

The PV and TEG arrays can be connected either in series or in parallel. The parallel connection may require additional unidirectional power electronic switches and a DC-DC converter for each array is probably mandatory for voltage constraints. In contrast, the series connection doesn't require additional power electronic switches and the number of series

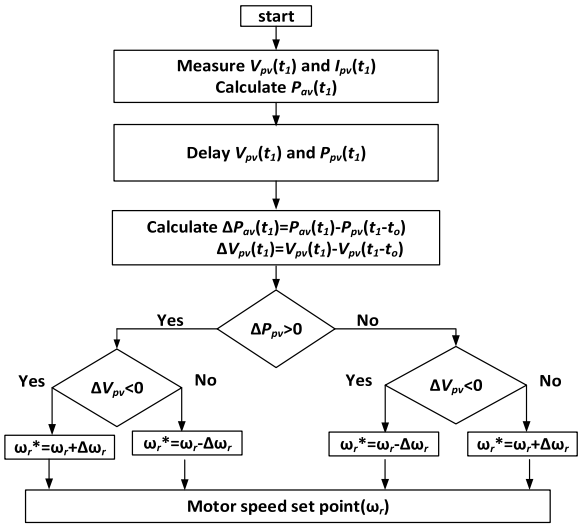

FIGURE 8. Schematic diagram of the perturbation and observation (P&O) MPPT scheme.

and parallel modules of both PV and TEG arrays can be selected and arranged optimally so that the motor inverter can be used to maximize the output power of the hybrid PV-TEG system. To do so, it is substantial to check the behavior of the PV and TEG arrays under the site conditions.

The following assumptions are used:

- Uniform irradiation level (IL) distribution over the whole PV modules;
- The ambient temperature (T) of the PV module is 30° C;
- The difference in the temperature (DT) of the TEG modules is 45°C.

The power rating of both PV and TEG arrays depends on the load requirements. Based on the design procedure mentioned in [14], [15], the peak power of the PV and TEG arrays are selected to be 5.034 kW and 404.70 W respectively. The ''KD135SX-UPU'' PV module type and the ''TE-MOD-1W2V-40S'' TEG module type are considered in this work. Clearly, the main source of the power is the PV array, which contributes by about 92% of the required rated load power. Thus, the arrangement of the series modules and parallel strings of the PV modules to achieve the requirements of the motor voltage and current is necessary. Consequently, the number of series and parallel modules of the PV array is 42 and 1 respectively. Figures 10 and 11 show the power and voltage versus the current of the PV array at various irradiation levels and at an ambient temperature of 30° C. The maximum power locus is depicted in both figures and clearly demonstrates the linear variation between the current and the maximum power of each irradiation level. The reason is that the voltage of the array is approximately constant at the maximum power point for the different irradiation levels as seen in Figure 11. Consequently, the MPPT can be done based on the PV array so that the maximum power locus of Figure 10 can be achieved, and then the series and parallel arrangements of the TEG modules can be done based on the maximum power locus of the PV array as will be shown hereafter.

The number of the TEG modules to achieve the required power (404.7 W) is 1000. Four series and parallel connections are possible for this number of modules to achieve a maximum power of 404.7 W. This is reported in Figures 12 and 13 that show the power and voltage versus current at various series and parallel connections and at a temperature different of 45 °C respectively. It is evident that the maximum current limit depends on the number of parallel strings. It is necessary that the maximum current limit of the TEG array is not lower than the maximum current of the maximum power locus of the PV array i.e. 7.63 A. This can be achieved by two connections: either using 25 series modules and 40 parallel strings or 50 series modules and 20 parallel strings. However, the output power of the TEG array varies based on the current flowing through it. This current is the current of the PV array at the maximum power point, which varies based on the irradiation level as seen in Figure 10. Therefore, the 50 series modules and 20 parallel strings connection is the optimal selection.

The output power versus the current of this TEG array is shown in Figure 14, with indicating the values of the power and current for 4 irradiation levels i.e. 250 W/m^2, 500 W/m^2, 750 W/m^2 and 1000 W/m^2. It is evident from Figure 10 that when the irradiation level varies from 1000 W/m^{2}to 250 W/m^2, the PV array output power reduces by about 78%. However, the output power of the TEG array reduces by about 56%. This means that the reduction is even low at higher irradiation levels: for example, it is about 4.5% when the irradiation level varies from 1000 W/m^{2}to 750 W/m^2. This proves that there is no need to complicate the system and increase the cost using the conventional methods of maximizing the PV-TEG hybrid system. The proposed method in this paper could be considered valuable.

V. PERFORMANCE OF THE PROPOSED SYSTEM

The mathematical model presented in section II, the control system shown in section III and the details of the PV-TEG hybrid system mentioned in section IV are used to simulate the performance of the whole system in MATLAB environment. Two cases are compared; in case 1, the motor is fed from only the PV array while in case 2 the motor is supplied from the hybrid PV-TEG system. The assumptions mentioned in section IV are applied. It is also assumed that the sun irradiation level is varied from 500 W/m^2 to 924 W/m^2. When the system is switched on, the MPPT starts to provide an initial set point for the motor speed. The motor starts to rotate. The MPPT increases the set point speed and compares the measured output power of the PV array at each time step with the previous step. Thereby, the motor speed increases as seen in Fig. 15 until the maximum output power of the PV array is achieved. Then, the motor speed becomes constant. Figure 15 shows the speed and torque of the motor as a function of time for the two cases. It is clear that the motor speed follows accurately the set point speed at the two irradiation levels. Further, the speed of the motor is higher by about 3.63% and 2.88% at IL = 500 W/m^2 and 924 W/m^2 respectively, when

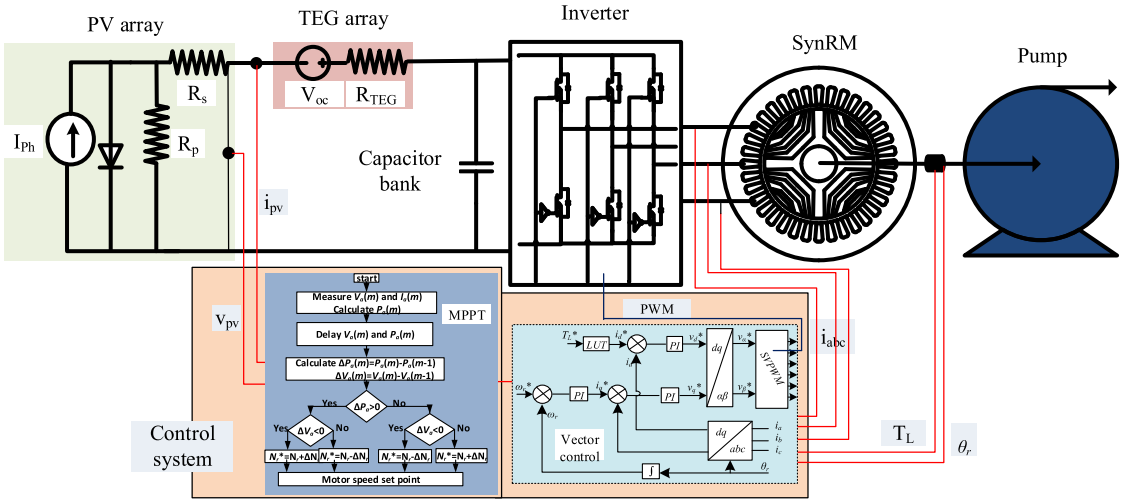

FIGURE 9. Schematic diagram of the whole system.

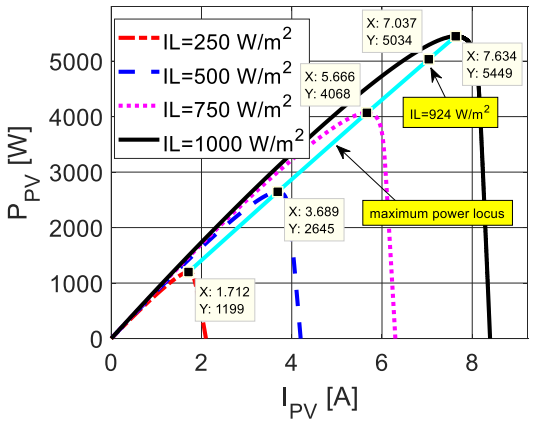

FIGURE 10. Output power versus current of the PV array at several irradiation levels and at T = 30°C.

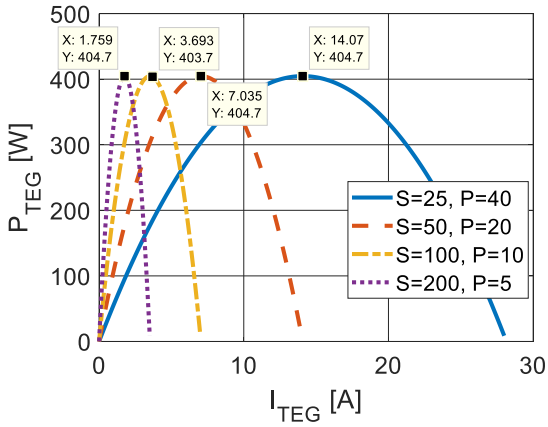

FIGURE 12. Output power versus current of the TEG array for various series (S) and parallel (P) connections and at TD = 45°C.

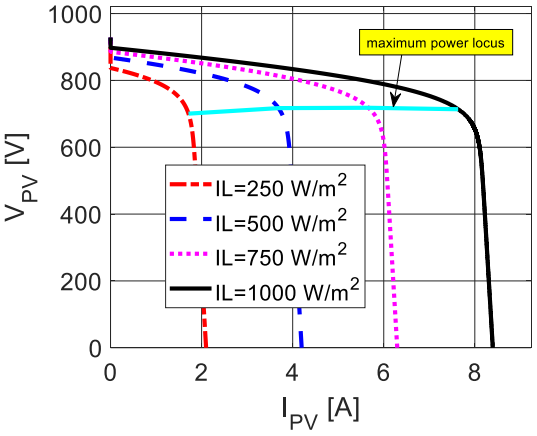

FIGURE 11. Output voltage versus current of the PV array at several irradiation levels and at T = 30°C.

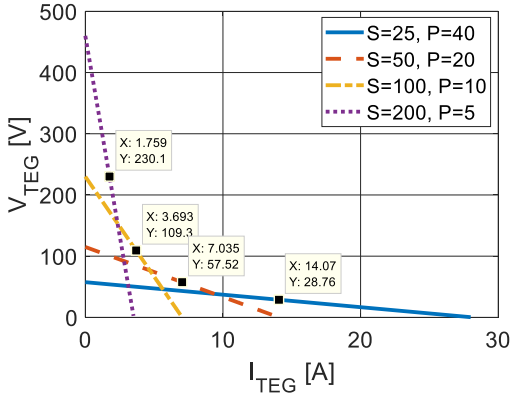

FIGURE 13. Output voltage versus current of the TEG array for various series (S) and parallel (P) connections and at TD = 45°C.

the hybrid PV-TEG array is used compared to the PV array. Consequently, the pump load torque is higher by about 6% and 5.7% respectively. This results in a higher output torque from the motor to cover the load torque. Eventually, the motor output power is increased by about 9.5% and 8.5% at IL = 500 W/m^2 and 924 W/m^2 respectively.

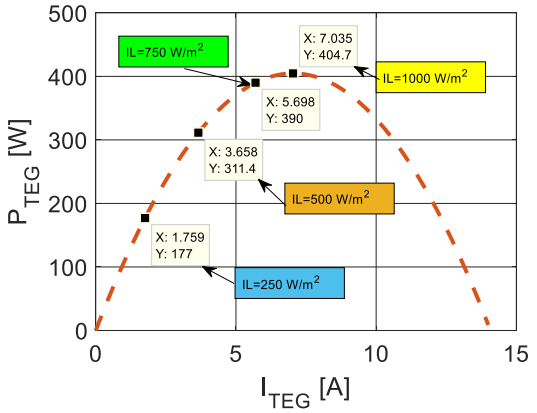

FIGURE 14. Output power versus current of the TEG array of 50 series modules and 20 parallel strings connection and at TD = 45°C.

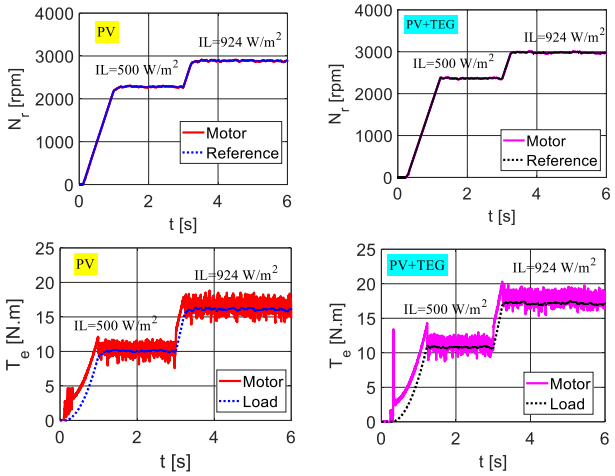

FIGURE 15. Response of speed and torque of the motor versus time at two irradiation levels (500 W/m^2 and 924 W/m^2).

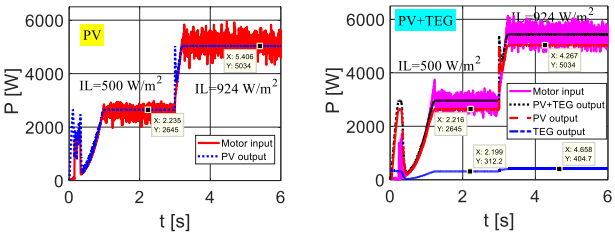

FIGURE 16. Power versus time of the motor and PV array at two irradiation levels (500 W/m^2 and 924 W/m^2).

Figure 16 reports the output power of the PV and PV-TEG arrays and the input power of the motor for the two irradiation levels i.e. IL = 500 W/m^2 and 924 W/m^2. It is obvious that the system works at the maximum power point of the PV array in the two cases, see Fig. 10. Further, the TEG array produces the maximum output power at IL = 924 W/m^2. However, when irradiation level moves away from 924 W/m^2, the TEG output power is not maximum. For example, when the irradiation level is 500 W/m^2, the output power of the TEG is reduced by about 23%, as seen in Figure 16, which

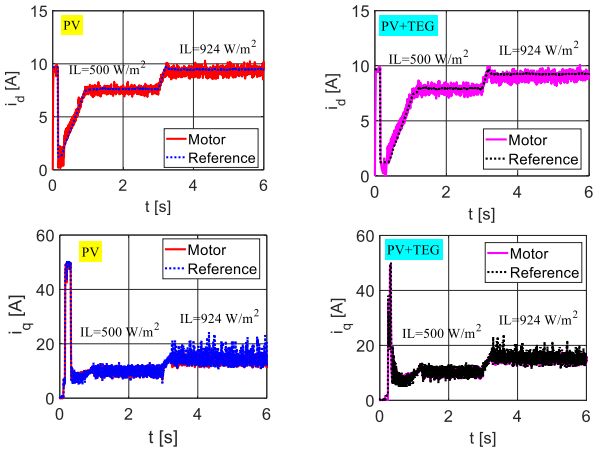

FIGURE 17. Motor current components of the motor versus time at two irradiation levels (500 W/m^2 and 924 W/m^2).

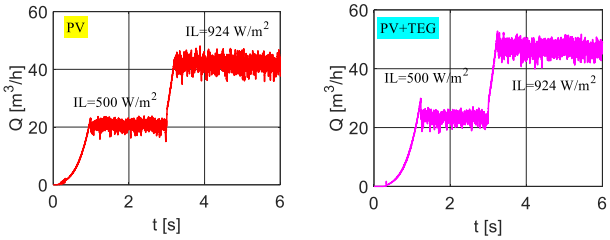

FIGURE 18. Pump flow rate versus time at two irradiation levels (500 W/m^2 and 924 W/m^2).

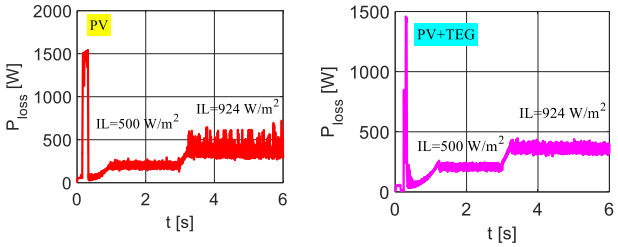

FIGURE 19. Motor losses of the motor versus time at two irradiation levels (500 W/m^2 and 924 W/m^2).

can be accepted situation for such high difference in irradiation level. Figure 17 shows the current components versus the time of the two cases. It evident that the current is similar in both cases. The flow rate of the pump is shown in Fig. 18 for both cases at the two irradiation levels. It is observed that the flow rate of the pump increases by about 12% and 9% at IL = 500 W/m^2 and 924 W/m^2 respectively, when suing PV-TEG array compared to PV array. The motor losses are displayed in Fig. 19. As seen in Fig. 17 that the current is similar between the two cases (PV and PV+TEG), hence the copper losses are similar. However, due to the higher speed in case of PV-TEG array, the iron losses are slightly higher. The dominant losses in the SynRM are the copper losses. This results in a slight increase in the motor losses when using PV-TEG array as illustrated in Fig. 19. Figure 20 shows the efficiency of the motor for both

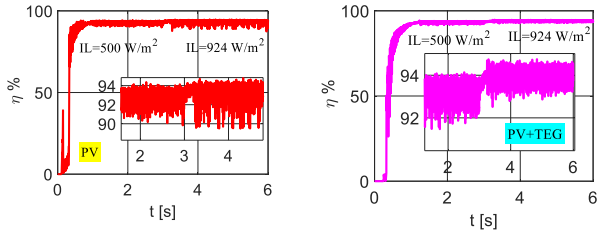

FIGURE 20. Motor efficiency (percentage value) of the motor versus time at two irradiation levels (500 W/m^2 and 924 W/m^2).

cases at the two irradiation levels. It is observed that the motor efficiency increases slightly in case of PV-TEG array: about 0.3%.

VI. EXPERIMENTAL VALIDATION

Experimental test bench is constructed to validate the theoretical work presented before. The test bench consists of the following main components: 1) 3-ph SynRM, of the specifications shown in Appendix section, fed from a SEMIKRON inverter, 2) 3-ph induction motor fed from a commercial inverter, 3) power analyzer to measure the voltage, current and power, 4) torque, speed and current sensors, 5) dSpace controller board and 6) a controlled (current, voltage and power) DC supply. The induction motor is controlled to emulate the characteristics of the pump load while the DC supply is employed to emulate the behavior of the hybrid PV-TEG array. A photograph of the complete test bench is depicted in Fig. 21.

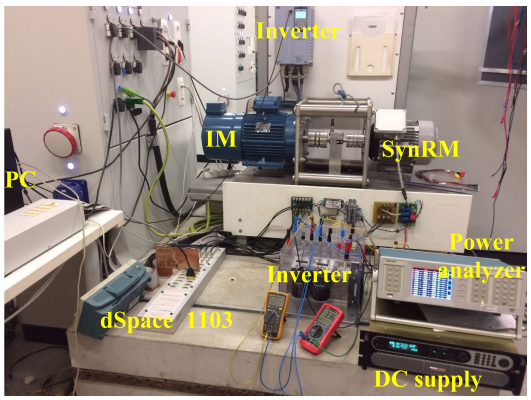

FIGURE 21. Experimental test bench.

The simulated results in case of PV-TEG array at IL = 924 W/m^2 presented before are validated by the measurements hereafter. Figure 22 shows the measured and set point of the motor speed. Figures 23 and 24 report the current components of the motor. It is clear that the motor follows accurately the set point values. The torque of the motor and load is shown in Figure 25. The measured torque corresponds well with the simulated result of Fig. 15. The measured efficiency map of the motor for torque and speed values up to the rated value is reported in Fig. 26. The working simulated point is depicted in the Figure as "Point". The measured

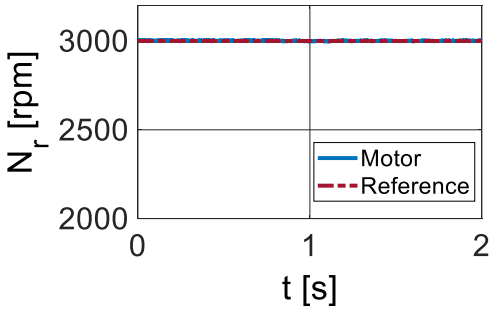

FIGURE 22. Measured motor speed versus time.

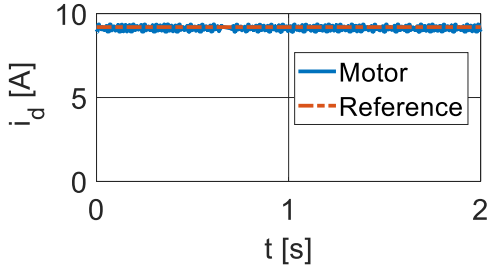

FIGURE 23. Measured motor current component of d-axis versus time.

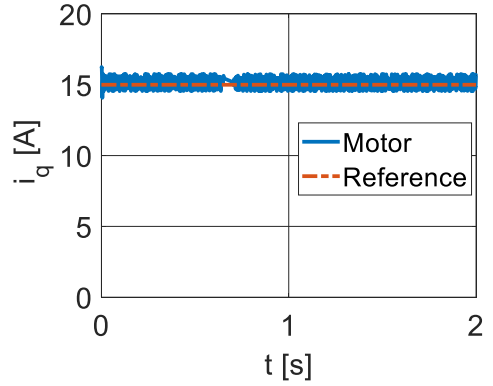

FIGURE 24. Measured motor current component of q-axis versus time.

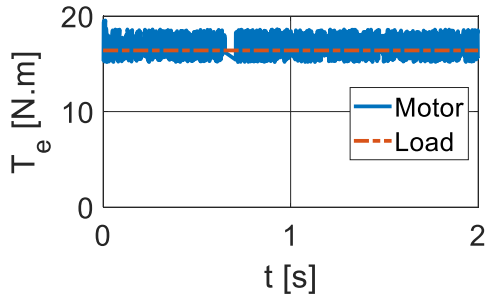

FIGURE 25. Measured torque of motor and reference load value versus time.

efficiency value is about 2% lower than that obtained from the simulation, see Fig. 20. Several reasons can lead to this difference among them the mechanical and PWM losses that are neglected in the simulation while they are inherently included in the measurements.

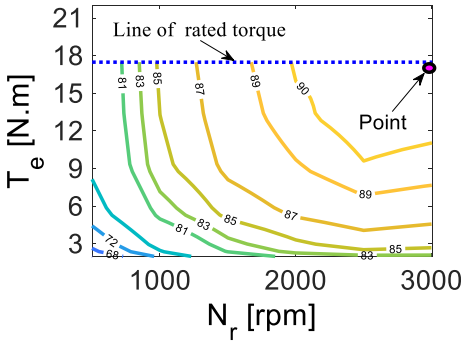

FIGURE 26. Measured motor efficiency map up to rated torque and speed.

VII. CONCLUSION

In this paper, a hybrid Photovoltaic (PV) -Thermoelectric Generator (TEG) system fed synchronous reluctance motor for pumping applications is presented. The system has neither DC-DC converters nor batteries. In addition, instead of using cooling system to cool the PV modules, the TEG modules are used that convert the heat generated by the PV modules into electric energy. Moreover, proposed control strategy is presented to drive the system in an appropriate way by controlling the motor inverter. It is observed that the motor output power and the pump flow rate are increased by about 9.5% and 12% respectively when using the hybrid PV-TEG array compared to only using PV array. Eventually, the whole system performance and cost are improved. Experimental measurements are obtained to validate the simulation results. The results prove the potential of using hybrid PV-TEG system driving SynRM for pumping applications.

APPENDIX

The SynRM parameters are as listed in Table 1.

TABLE 1. SynRM parameters.

Variable	Value	Variable	Value
Stator slots/ poles	36/4	Stack length	140 mm
Flux barriers /pole	3	Rotor /stator steel	M330-50A/ M270-50A
Number of phases	3	Length of air gap	0.3 mm
Outer /inner diameter of the stator	180 mm/ 110 mm	Rated voltage/ current	380 V/12.23 A
Shaft diameter	35 mm	Rated power	5.5 kW
Outer diameter of the rotor	109.4 mm	Rated speed	3000 rpm

REFERENCES

[1] V. Verma, A. Kane, and B. Singh, "Complementary performance enhancement of PV energy system through thermoelectric generation," *Renew. Sustain. Energy Rev.*, vol. 58, pp. 1017–1026, May 2016.

[2] V. V. Tyagi, N. A. A. Rahim, N. A. Rahim, and J. A. L. Selvaraj, "Progress in solar PV technology: Research and achievement," *Renew. Sustain. Energy Rev.*, vol. 20, pp. 443–461, Apr. 2013.

[3] B. Parida, S. Iniyan, and R. Goic, "A review of solar photovoltaic technologies," *Renew. Sustain. Energy Rev.*, vol. 15, no. 3, pp. 1625–1636, 2011.

[4] F. Attivissimo, A. Di Nisio, A. M. L. Lanzolla, and M. Paul, "Feasibility of a photovoltaic–thermoelectric generator: Performance analysis and simulation results," *IEEE Trans. Instrum. Meas.*, vol. 64, no. 5, pp. 1158–1169, May 2015.

[5] C. Babu and P. Ponnambalam, "The theoretical performance evaluation of hybrid PV-TEG system," *Energy Convers. Manage.*, vol. 173, pp. 450–460, Oct. 2018.

[6] M. Hasanuzzaman, A. B. M. A. Malek, M. M. Islam, A. K. Pandey, and N. A. Rahim, "Global advancement of cooling technologies for PV systems: A review," *Solar Energy*, vol. 137, pp. 25–45, Nov. 2016.

[7] J. Lin, T. Liao, and B. Lin, "Performance analysis and load matching of a photovoltaic–thermoelectric hybrid system," *Energy Convers. Manage.*, vol. 105, pp. 891–899, Nov. 2015.

[8] B. Subudhi and R. Pradhan, "A comparative study on maximum power point tracking techniques for photovoltaic power systems," *IEEE Trans. Sustain. Energy*, vol. 4, no. 1, pp. 89–98, Jan. 2013.

[9] S. Lyden and M. E. Haque, "Maximum Power Point Tracking techniques for photovoltaic systems: A comprehensive review and comparative analysis," *Renew. Sustain. Energy Rev.*, vol. 52, pp. 1504–1518, Dec. 2015.

[10] M. Arrouf and N. Bouguechal, "Vector control of an induction motor fed by a photovoltaic generator," *Appl. Energy*, vol. 74, nos. 1–2, pp. 159–167, Jan. 2003.

[11] K. Benlarbi, L. Mokrani, and M. S. Nait-Said, "A fuzzy global efficiency optimization of a photovoltaic water pumping system," *Sol. Energy*, vol. 77, no. 2, pp. 203–216, 2004.

[12] M. Nabil, S. M. Allam, and E. M. Rashad, "Modeling and design considerations of a photovoltaic energy source feeding a synchronous reluctance motor suitable for pumping systems," *Ain Shams Eng. J.*, vol. 3, no. 4, pp. 375–382, Dec. 2012.

[13] M. Nabil, S. M. Allam, and E. M. Rashad, "Performance improvement of a photovoltaic pumping system using a synchronous reluctance motor," *Electr. Power Compon. Syst.*, vol. 41, no. 4, pp. 447–464, Feb. 2013.

[14] M. N. Ibrahim, P. Sergeant, and E. M. Rashad, "Design of low cost and efficient photovoltaic pumping system utilizing synchronous reluctance motor," in *Proc. IEEE Int. Electr. Mach. Drives Conf. (IEMDC)*, Miami, FL, USA, May 2017, pp. 1–7.

[15] M. N. Ibrahim, H. Rezk, M. Al-Dhaifallah, and P. Sergeant, "Solar array fed synchronous reluctance motor driven water pump: An improved performance under partial shading conditions," *IEEE Access*, vol. 7, pp. 77100–77115, 2019.

[16] R. Kumar and B. Singh, "Single stage solar PV fed brushless DC motor driven water pump," *IEEE J. Emerg. Sel. Topics Power Electron.*, vol. 5, no. 3, pp. 1377–1385, Sep. 2017.

[17] P. Packiam, N. K. Jain, and I. P. Singh, "Steady and transient characteristics of a single stage PV water pumping system," *Energy Syst.*, vol. 6, no. 2, pp. 173–199, Jun. 2015.

[18] A. B. Raju, S. R. Kanik, and R. Jyoti, "Maximum efficiency operation of a single stage inverter fed induction motor PV water pumping system," in *Proc. 1st Int. Conf. Emerg. Trends Eng. Technol.*, Jul. 2008, pp. 905–910.

[19] M. N. Ibrahim, P. Sergeant, and E. M. Rashad, "Relevance of including saturation and position dependence in the inductances for accurate dynamic modeling and control of SynRMs," *IEEE Trans. Ind. Appl.*, vol. 53, no. 1, pp. 151–160, Jan./Feb. 2017.

[20] M. N. F. Ibrahim, A. S. Abdel-khalik, E. M. Rashad, and P. Sergeant, "An improved torque density synchronous reluctance machine with a combined star–delta winding layout," *IEEE Trans. Energy Convers.*, vol. 33, no. 3, pp. 1015–1024, Sep. 2018.

[21] M. N. Ibrahim, P. Sergeant, and E. M. Rashad, "Combined star-delta windings to improve synchronous reluctance motor performance," *IEEE Trans. Energy Convers.*, vol. 31, no. 4, pp. 1479–1487, Dec. 2016.

[22] M. N. F. Ibrahim, E. Rashad, and P. Sergeant, "Performance comparison of conventional synchronous reluctance machines and PM-assisted types with combined star–delta winding," *Energies*, vol. 10, no. 10, p. 1500, Sep. 2017.

[23] X. Zhang, K. T. Chau, and C. C. Chan, "Design and implementation of a thermoelectric -photovoltaic hybrid energy source for hybrid electric vehicles," *World Electr. Veh. J.*, vol. 3, no. 2, pp. 0271–0281, 2009.

MOHAMED N. IBRAHIM received the B.Sc. degree in electrical power and machines engineering from Kafrelshiekh University, Egypt, in 2008, the M.Sc. degree in electrical power and machines engineering from Tanta University, Egypt, in 2012, and the Ph.D. degree in electromechanical engineering from Ghent University, Belgium, in 2017. In 2008, he became a Teaching Assistant with the Electrical Engineering Department, Kafrelshiekh University. He is currently working as a Postdoctoral Researcher with the Department of Electrical Energy, Metals, Mechanical Constructions and Systems, Ghent University, Belgium. He is also an Assistant Professor with the Department of Electrical Engineering, Kafrelshiekh University. His major research interest includes design and control of electrical machines and drives for industrial and sustainable energy applications. He received the Kafrelshiekh University Award for his international scientific publications for several times.

HEGAZY REZK received the B.Eng. and M.Eng. degrees in electrical engineering from Minia University, Egypt, in 2001 and 2006, respectively, and the Ph.D. degree from the Moscow Power Engineering Institute, Moscow. He was a Postdoctoral Research Fellow with the Moscow State University of Mechanical Engineering, Russia, for six months. He was a Visiting Researcher with Kyushu University, Japan, for one year. He is currently an Associate Professor with the Electrical Engineering Department, Collage of Engineering, Wadi Addwaser, Prince Sattam University, Saudi Arabia. He has authored more than 50 technical articles. His current research interests include renewable energy, smart grid, hybrid systems, power electronics, optimization, and artificial intelligence.

MUJAHED AL-DAHIFALLAH received the B.Sc. and M.Sc. degrees in systems engineering from the King Fahd University of Petroleum and Minerals, Dhahran, Saudi Arabia, and the Ph.D. degree in electrical and computer engineering from the University of Calgary, Calgary, AB, Canada. He has been an Assistant Professor of systems engineering with the King Fahd University of Petroleum and Minerals, since 2009. His current research interests include nonlinear systems identification, control systems, optimization, artificial intelligence, and renewable energy.

PETER SERGEANT received the M.Sc. degree in electromechanical engineering, and the Ph.D. degree in engineering sciences from Ghent University, Ghent, Belgium, in 2001 and 2006, respectively, where he is currently a Professor in electrical drives, and also the Core Lab Manager in the cluster Motion Products of Flanders Make. In 2001, he became a Researcher with the Electrical Energy Laboratory, Ghent University. He became a Postdoctoral Researcher with Ghent University, in 2006 (Postdoctoral Fellow of the Research Foundation - Flanders). Since 2012, he has been an Associate Professor with Ghent University. His current research domain is electrical machines and drives for industrial and for sustainable energy applications. The focuses are on accurate computation of losses in machines and drives, improving energy efficiency, and increasing power density.